J Mater Sci (2007) 42:1872–1883
DOI 10.1007/s10853-006-1316-9

NONSTOICHIOMETRIC COMPOUNDS

Active anion manipulation for emergence of active functions in the nanoporous crystal $12CaO \cdot 7Al_2O_3$: a case study of abundant element strategy

Hideo Hosono · Katsuro Hayashi · Masahiro Hirano

Received: 31 October 2005 / Accepted: 1 March 2006 / Published online: 9 January 2007

Abstract This article reviews our approach to render $12CaO \cdot 7Al_2O_3$ (C12A7) electronically active using a new concept of 'active anion manipulation', where nanostructures embedded within the C12A7 crystal lattice are intentionally utilized to generate chemically unstable ('water-free active') anions. Anionic active oxygen radicals, O^- and O_2^-, are formed efficiently in C12A7 cages under high oxygen activity conditions. The configuration and dynamics of O_2^- in cages are revealed by a combination of continuous-wave and pulsed electron paramagnetic resonance (EPR). It is demonstrated that metal-loaded C12A7 is a promising oxidation catalyst for syngas ($CO + H_2$) formation from methane. Furthermore, the O^- ion, the strongest oxidant among active oxygen species, can be extracted from the cage into an external vacuum by applying an electric field with thermal assistance, generating a high-density O^- beam in the order of $\mu A\ cm^{-2}$. In contrast, heat treatment of C12A7 in a hydrogen atmosphere forms H^- ions in the cages. The resultant C12A7:H^- exhibits a persistent insulator-conductor conversion upon ultraviolet-light or electron-beam irradiation. The irradiation-induced conversion mechanism is examined by first-principle theoretical calculations. Furthermore, the presence of a severely reducing environment causes the complete substitution of electrons for anions in the cages. The resulting C12A7:e^-, which exhibits excellent stability and an electrical conductivity greater than 100 S cm^{-1}, is regarded as an 'electride', an ionic compound in which electrons serve as anions. The C12A7 electride exhibits a high potential for applications involving cold cathode and thermal field electron emissions due to its small work function. Electride fabrication methods suitable for large-scale production via melt processing are described. It is also demonstrated that proton or inert gas ion implantations into C12A7 thin films at elevated temperatures are effective for both H^- and electron doping.

H. Hosono (✉) · K. Hayashi · M. Hirano
Frontier Collaborative Research Center, Tokyo Institute of Technology, S2-13, 4259 Nagatsuta, Yokohama 226-8503, Japan
e-mail: hosono@msl.titech.ac.jp

Introduction

$12CaO \cdot 7Al_2O_3$ (C12A7), commonly known as the mineral 'mayenite', is produced on a large-scale for use in industry as a constituent of alumina cements. Although C12A7 appears only to have passive functions only useful for structural material purposes, it in fact has huge potential for exhibiting active functionalities if its distinct crystal structure is fully utilized. The unit cell of C12A7 contains two molecules and may be expressed as $[Ca_{24}Al_{28}O_{64}]^{4+} + 2O^{2-}$. The $[Ca_{24}Al_{28}O_{64}]^{4+}$ component denotes a three-dimensional lattice framework, containing 12 cages with an inner free space of ~0.4 nm diameter, as illustrated in Fig. 1. Each cage has a mean effective charge of +1/3 (= +4 charges/12 cages) [1], and is connected to its eight nearest neighbor cages via ~0.1 nm-wide-openings. The transport of encaged ionic or electrically conductive species may take place through this small opening. The remaining $2O^{2-}$ component is referred to as 'free oxygen' or 'extra-framework oxide ions', and

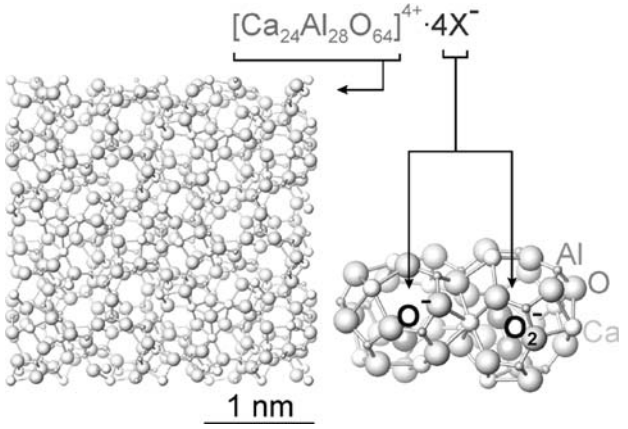

Fig. 1 Crystal structure of C12A7 (space group: I $\bar{4}$3d and lattice constant: ~12 nm) viewed from the <111> direction, revealing cages for the incorporation of anions (O^- and O_2^-). Since the lattice framework is positively charged (+1/3 per cage), the electroneutrality is preserved by the incorporation of anions into the cages

occupies 1/6 of the cage sites. The oxide ions can be partially or completely replaced by various monovalent anions such as OH^- [2], F^-, and Cl^- [3]. Such anion-exchange properties are complementary to conventional natural nanoporous crystals, e.g., zeolites, whose lattice framework is negatively charged and formed with extra-framework cations.

The incorporation of unconventional anions into C12A7 cages was first reported by Hosono and Abe [4], who found superoxide ions (O_2^-) at a concentration of $\sim 1 \times 10^{19}\,cm^{-3}$ in C12A7 polycrystalline samples prepared under ambient conditions. This finding stimulated an examination of the ionic conduction properties of oxygen-related anions in C12A7, leading to the discovery of fast O^{2-} ion conduction [5]; a phenomenon believed to be due to the 'free oxygen'. It is also noteworthy that C12A7 readily forms a glass phase, and under oxidizing conditions the formed glass contains ozonide ion (O_3^-) and aluminum-oxygen hole centers (Al–OHC) [6]. On the other hand, F^+-like centers are produced in a glass fabricated in reducing atmosphere on exposure to ultraviolet (UV)-light. The formation of F^+-like centers change color of the glass, which is restored near room temperature after the illumination is stopped [7]. The photosensitivity of C12A7 glass totally differs from that of well-known photosensitive/photochromic glasses in that it emerges without doping the glass with optically active cations such as Au and Ag.

Our approach to render C12A7 electro-active is based on the incorporation of chemically unstable (i.e., 'active') negative species into the inherently positively-charged C12A7 cage by chemical (thermal treatment in a suitable atmosphere) and physical (ion implantation) processes. We also employ a combination of conventional and state-of-the-art characterization techniques, including optical absorption, transient photoluminescence, Raman spectroscopy, thermogravimetric-mass spectroscopy (TG-MS), photoelectron spectroscopy, and continuous and pulsed electron paramagnetic resonance (EPR) for the characterization of the encaged anions. Such comprehensive characterization allows for a better understanding of the various novel phenomena discovered in C12A7 [8, 9].

In addition, various forms of C12A7 samples are needed to advance our understanding of this interesting nanoporous material, as well as to cultivate the full application potential of C12A7. In particular, single crystals of C12A7 is indispensable for exploring novel functions of C12A7, such as UV light-induced electrical conductivity, the synthesis of an electride, and the clarification of the oxygen radical configuration in the cage. Furthermore, the role of theoretical analysis in providing clear physical and chemical insights for understanding the novel phenomena in C12A7 is equally important. Indeed, the use of ab-initio quantum mechanical calculations that incorporate a structural relaxation will be indispensable for addressing the 'soft' framework of C12A7; a structure which deforms considerably when an anion or an electron is incorporated within the cage.

Synthesis of various C12A7 shapes

Translucent ceramics

Fully densified translucent C12A7 ceramics were obtained by sintering hydrated C12A7 powders in a dry oxygen atmosphere at 1300 °C; where a dry atmosphere enhances the densification much better than a wet atmosphere. The average transmittance between 400–800 nm for 1 mm thick samples was improved up to ~70% by sintering for 48 h. The elimination of water molecules existing in triple grain boundaries is likely to play a crucial role in improving the transparency [10].

Single crystals

The fabrication of C12A7 single crystals using the conventional floating zone method produced a concave solid–liquid interface, which resulted in the formation of many bubbles and cracks in the grown crystals. By lowering the growth rate to 1 $mm \cdot h^{-1}$, it was possible to significantly reduce bubble generation. Here, suppression

of the bubbles is very important, because their formation disturbs the stability of the molten zone. Introducing an alumina tube into the heating zone produced more uniform temperatures, such that a convex solid–liquid interface could be formed. A convex solid–liquid interface enabled the growth of high-quality crystals with higher growth rates [11].

Thin films

Polycrystalline C12A7 thin films were prepared by room-temperature deposition of amorphous C12A7 films on MgO substrates by pulsed laser deposition (PLD), followed by thermal annealing of the films in an oxygen atmosphere at temperatures above 800 °C [12].

Incorporation of active oxygen species

Oxygen radical formation

It was found that extraordinarily high concentrations of oxygen radicals (O^- and O_2^-) on the order of 10^{20} cm^{-3} could be formed in the C12A7 cages simply by heating the C12A7 ceramics in a dry oxygen atmosphere [13]. The concentrations of O_2^- and O^- were evaluated through a combination of electron paramagnetic spin resonance (EPR) and Raman spectroscopy. The resultant C12A7 exhibited outstanding oxidative reactivity, such that even Pt metal could be oxidized into the +4 state when the metal was contacted with the material at high temperatures. The effect of oxygen partial pressure (up to 400 atm) on the generation of active oxygen radicals was examined using a hot isostatic-pressing furnace. The total concentration of active oxygen radicals was observed to increase with oxygen partial pressure up to 1.7×10^{21} cm^{-3}, which is comparable to the theoretical maximum concentration of monovalent anions in cages, 2.3×10^{21} cm^{-3} [14].

The formation of oxygen radicals was markedly reduced as the water vapor pressure increased due to the formation of OH^- ions in the cages [15]:

$$O^{2-}\ (\text{cage}) + H_2O\ (g) \rightarrow 2OH^-\ (\text{cage}). \quad (1)$$

The formation of oxygen radicals in a dry oxygen atmosphere is attributed to the absorption of oxygen molecules into C12A7, where the dominant reaction is most likely:

$$O^{2-}\ (\text{cage}) + O_2\ (g) \rightarrow O^-\ (\text{cage}) + O2^-\ (\text{cage}). \quad (2)$$

The formation of oxygen radicals (O^- or O_2^-) causes an excess of oxygen with respect to the stoichiometric composition of C12A7. The excess oxygen desorbs when heated empirically to ~700 °C in an inert atmosphere [16, 17]. The evaluation of the enthalpy and entropy of radical formation in Eq. 2 enables us to determine the temperature and oxygen partial pressure dependences of the equilibrium oxygen radical concentration (Fig. 2). The rate-limiting processes for radical formation are not the surface reactions, but rather the bulk chemical diffusion of oxygen, in which the diffusion of O_2^- most likely dominates the total process [18]. These results allow one to predict the total oxygen radical content for a given annealing condition [19]. The validity of Eq. 2 was further verified by ESR measurements on a C12A7 single crystal heated in an $^{17}O_2$ isotope gas [20], as will be described in the following section.

Configuration and dynamics of O_2^- radicals in cages

The physical state of the O_2^- ion in C12A7 was studied by continuous-wave and pulsed EPR [20]. A C12A7 single crystal heated in 40% ^{17}O-enriched gas showed a hyperfine splitting due to the $^{17}O_2^-$ ion. This fact clearly indicates that the O_2^- ion is formed via the reaction between an atmospheric O_2 molecule and an extra-framework O^{2-} ion, as given by Eq. 2. The angular variations of the *g*-values and ^{17}O hyperfine splitting were measured for the single crystal at 20 K, while ^{27}Al-electron spin-echo envelope modulation (ESEEM) powder patterns were measured at 4 K. These results verified that the O_2^- radical is located inside the cage, being adsorbed on the Ca^{2+} ions of the cage wall. Furthermore, the configuration of the O_2^- ion

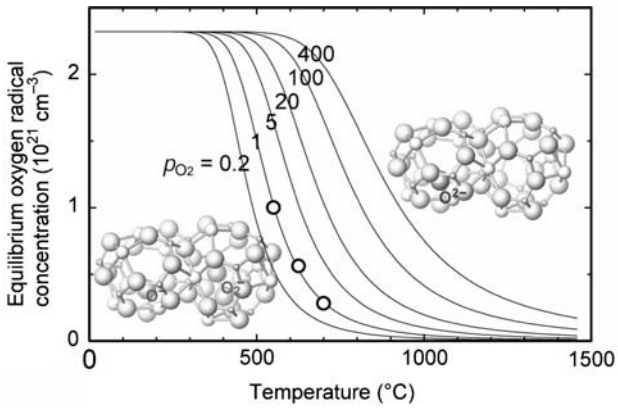

Fig. 2 Oxygen partial pressure and temperature dependences of oxygen radical concentration at equilibrium. Circles denote measured equilibrium concentrations

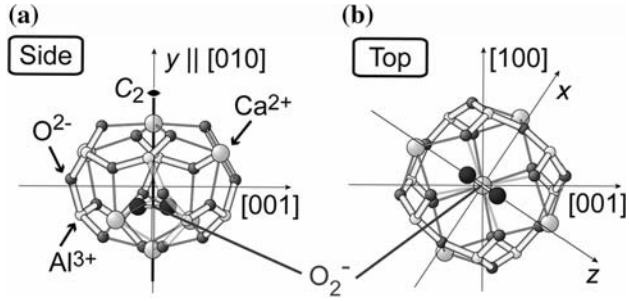

Fig. 3 Crystallographic configuration of the O_2^- ion inside the C12A7 cage determined from an EPR study: (**a**) side view, and (**b**) top view

is determined such that two constituent oxygen atoms occupy crystallographically equivalent sites within the cage. The O_2^- ion bonds to the Ca^{2+} ion via a 'side-on' configuration, where the O–O bond is perpendicular to the two-fold rotational axis (C_2//<100>) of the cage, and is directed towards other two calcium ions in the cage wall (Fig. 3).

The dynamic motion of the O_2^- ion was clarified from the temperature dependence of the *g*-values: the O_2^- ion stays at a fixed position without noticeable movement, behaving like a 'solid' below ~20 K, forming a 'glass state', such that the swinging rotation of the O–O bond along the C_2 axis is activated with temperature. The anisotropy in the swinging motion disappears above ~400 K, making the O_2^- ion state 'liquid-like'. These results may be explained in terms of the electrostatic interaction between the Ca^{2+} ion and π-orbital of the O_2^- radicals.

Partial oxidation of methane into syngas

The partial oxidation of methane into syngas (CO and H_2) was examined using C12A7 powders, promoted by metal catalysts (M) such as Ni, Co, Pt, Pd, and Ru [21]. The catalytic ability of M/C12A7 was examined and compared with the activity of a nickel catalyst supported on either CaO, α-Al_2O_3, or calcium aluminates with a high CaO/Al_2O_3 ratio. On Ni, Pt, and, Pd/C12A7, the reaction took place readily at temperatures as low as 500 °C, and reached thermodynamic equilibrium quickly. The catalytic activity of M/C12A7 is in the order of Pt/C12A7 (1% Pt loaded > Co/C12A7 (5%) > Ni/C12A7 (5%) > Ru/C12A7 (1%) > Pd/C12A7 (1%) for a space velocity of 240,000 ml g^{-1} h^{-1} at 800 °C. Large increases in the activity and selectivity for syngas formation were observed for the Ni/C12A7 and Pt/C12A7 catalysts. These systems were found to be more catalytically active than nickel supported on either CaO, α-Al_2O_3, $3CaO{\cdot}Al_2O_3$ (C3A), or $CaO{\cdot}Al_2O_3$ (CA) (Fig. 4). This enhanced activity of Ni over other metals may be attributed to the good dispersion of NiO on C12A7.

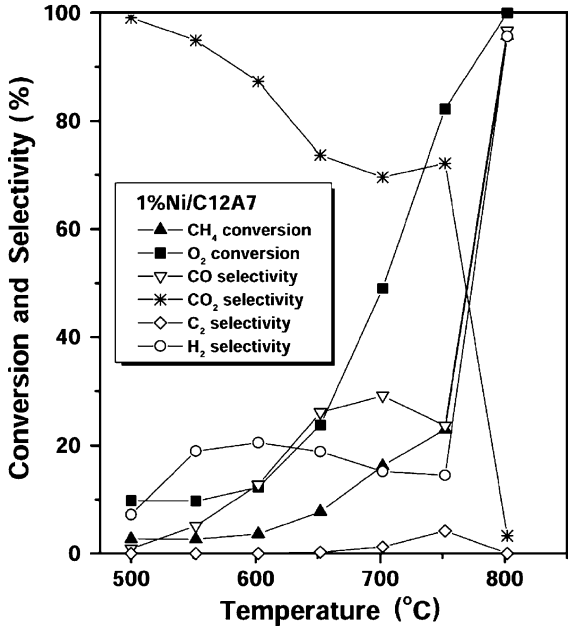

Fig. 4 Conversion efficiency of the initial mixed gas (CH_4 and O_2) and selectivity of reaction products (CO, CO_2, C_2 and H_2) as a function of temperature in the partial oxidation of CH_4 using 1% Ni/C12A7 as a catalyst. Gas space velocity was 30,000 ml $g^{-1}h^{-1}$

Generation of O^- ion beam

By applying a DC voltage to a C12A7 cage containing a large amount of O^- (1×10^{20} cm^{-3}) and O_2^- (3×10^{20} cm^{-3}), it was possible to selectively extract O^- ions to form an intense pure O^- ion beam [22–25]. Using a sample temperature of 800 °C and an applied electric voltage greater than 1 kV cm^{-1}, the resulting O^- current density was observed to increase to ~2 μA cm^{-2}, which is higher than the maximum value obtained from yttria-stabilized zirconia (YSZ) by three orders of magnitude (Fig. 5). Moreover, unlike YSZ, which requires a surface metal electrode to dissociate surface O^{2-} ions into a pair of O^- radicals and an electron, here O^- ions can be extracted from the as-prepared C12A7 surface without the use of additional electrodes. The presence of extremely large concentrations of O^- and O_2^- radical ions, coupled with the fast oxide ion conductive nature of C12A7, allows for the extraction of O^- radicals directly from the C12A7 surface. The generation of a high-density O^- ion current is applicable to various novel oxidation processes, such as the formation of gate dielectrics on semiconductors, organic chemical reactions, the

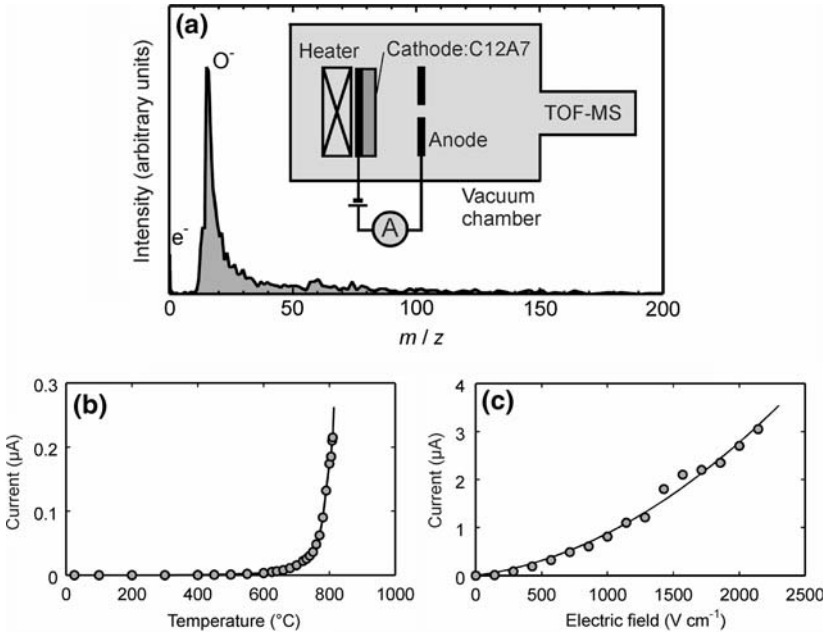

Fig. 5 Emission of O^- ions from C12A7. (**a**) Typical time-of-flight mass spectrum of an ion current extracted from C12A7. Inset is a schematic drawing of the O^- beam generation equipment. (**b**) Ion current (composed primarily of O^- ions) obtained between two electrodes as a function of sample temperature for an extracting DC voltage of 375 V. (**c**) Ion current emitted from a C12A7 disk of 2 cm^2 area as a function of applied DC voltage at 810 °FC

decomposition of pollutants, and sterilization. Therefore, the development of a continuous O^- beam generation system using a C12A7 ceramic membrane is a certain target for future research.

Incorporation of H^- ions

Photoinduced conversion of C12A7:H^- from insulator to conductor

Electronic conduction in light metal oxides was first realized in C12A7 back in 2002 [26]. Here, hydride ions (H^-) were incorporated into the C12A7 cages by thermal treatment in a hydrogen atmosphere. The as-treated C12A7:H^- is colorless and a good insulator with an electronic conductivity of less than 10^{-10} S cm^{-1}. However, upon illumination with UV light, the C12A7:H^- is converted into a yellowish green electronic conductor with a conductivity of 0.3 S cm^{-1} at 300 K (Fig. 6). The conductive state of C12A7:H^- is preserved even after the irradiation is stopped. However, when heated above ~300 °C, C12A7:H^- reverts back to an insulator, and the optical absorption intensities decay concomitantly. Heating C12A7:H^- above ~550 °C causes the release of H_2 gas and a concomitant loss of photosensitivity. Upon UV light illumination, the H^- ions emit electrons trapped within the cages, resulting in the formation of F^+-like centers as will be discussed later. Their migration is responsible for the electrical conduction.

UV-illumination of H^--accommodating C12A7 thin films also results in conversion of C12A7:H^- from an insulator to a conductor. Here, H^- ions are formed either by thermal treatment in a hydrogen atmosphere at 1200 K or via the hot ion implantation of H^+ ions into C12A7 [27], as will be described later. The visible light absorption loss is estimated to be only 1% for 200 nm-thick C12A7:H^- films with an electrical conductivity of 1 S cm^{-1} at 300 K (Fig. 7). These properties enable novel applications such as the direct optical writing of transparent electronic circuits on insulating media.

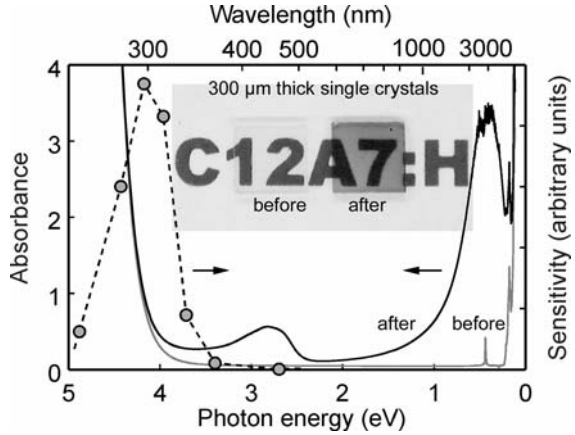

Fig. 6 Optical absorption spectra for a H^--loaded C12A7 single crystal before (gray line) and after (black line) illumination with UV light. Circles denote the photon energy dependence of the sensitivity on the coloration. Inset is a photograph of C12A7:H^- single crystals before and after UV illumination

The generation of persistent carrier electrons in C12A7:H^- by electron-beam irradiation was also examined [28]. The surface layer of an insulating

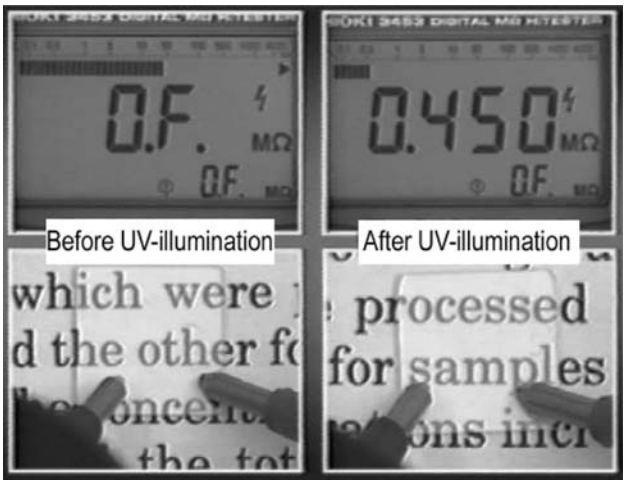

Fig. 7 Photoinduced conduction in H^--loaded C12A7 thin films. Both electrically insulating (lower left) and conductive (lower right) films appear colorless and transparent. The scales in the images show the electrical conductivity of each film

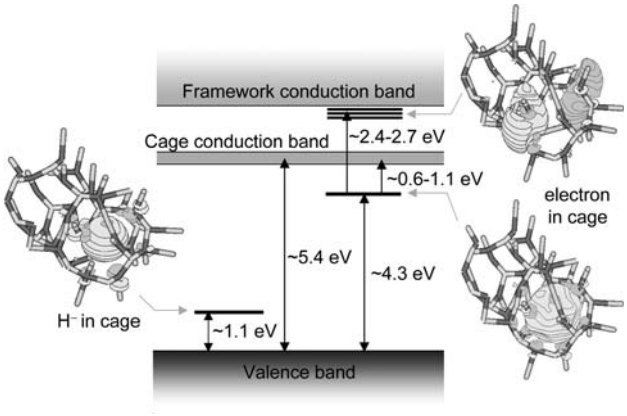

Fig. 8 A schematic of the energy levels in C12A7 incorporating either H^- ions or electrons, together with the corresponding wavefunctions obtained by first-principle calculations based on the embedded cluster approach. The excitation from the localized electronic state (F^+-like center) to the cage conduction band (~0.6–1.1 eV) corresponds to the inter-cage charge transfer transition. Excitations to the higher energy (2.4–2.7 eV) levels correspond to the intra-cage s–p transitions

C12A7:H^- single crystal was directly converted to an electronic conductor by electron-beam irradiation. Here, the observed green coloration is identical to that induced by UV-light irradiation. The carrier electron formation was saturated at an electron beam dose of 300 μC cm^{-2}, which is comparable to the sensitivity of conventional photoresists for electron-beam lithography. The yield of the carrier electron generation in C12A7:H^- per incident electron was estimated to be as high as 30 for an acceleration voltage of 25 keV.

Mechanism for photoinduced conversion

An embedded cluster approach was employed to calculate the electronic state of the extra electron doped into C12A7 (Fig. 8) [29–31]. Our results indicate that the empty cage state forms a narrow conduction band called a 'cage conduction band', which is located ~5.4 eV above the valence band (VB) and ~2 eV below the framework conduction band. When an electron is introduced into the cage, its energy level is lowered by ~1 eV from the empty cage conduction band due to lattice relaxation. As a result, the electron becomes localized in the cage in the same manner as an electron is localized in an anion vacancy in alkali halides or alkaline-earth oxides. Thus, such an electron center in C12A7 is termed an 'F^+-like center'. However, since each cage is connected directly to several other empty cages, electrons are able to hop to neighboring cages with activation energy of only ~0.1 eV. This electron hopping yields electrical conductivity, and as such, the extra-framework electron is regarded as a 'polaron'. In addition, the F^+-like center introduces two absorption bands with peaks at ~0.4 eV and ~2.8 eV (See Fig. 6). These bands are assigned to the inter-cage charge transfer and the intra-cage s–p transitions of the electron, respectively. Furthermore, theoretical calculations on both the ground and photoexcited states of C12A7:H^- confirm that the insulator-conductor conversion is induced by the photoionization of the H^- ion to form a pair of H^0 and an electron under illumination at ~4.3 eV [32]:

$$H^- \text{ (cage)} + \text{null (cage)} \rightarrow H^0 \text{ (cage)} + e^- \text{ (cage)}. \quad (3)$$

These theoretical analyses are consistent with experimental observations. However, no H^0 was detected by EPR at room temperature, suggesting that H^0 is so unstable that it may further decompose into H^+ and an electron. As such, the H^+ ions may form O–H bonds with framework O^{2-} ions. They can then diffuse along other framework O^{2-} ions, and eventually react with extra-framework O^{2-} ions to form OH^- ions:

$$H^0\text{(cage)} + O^{2-}\text{(framework)} \rightarrow O^{2-}\text{(framework)} - H^+ + e^- \text{ (cage)} \quad (4)$$

$$O^{2-}\text{(framework)} - H^+ + O^{2-}\text{(cage)} \rightarrow O^{2-}\text{(framework)} + OH^- \text{ (cage)} \quad (5)$$

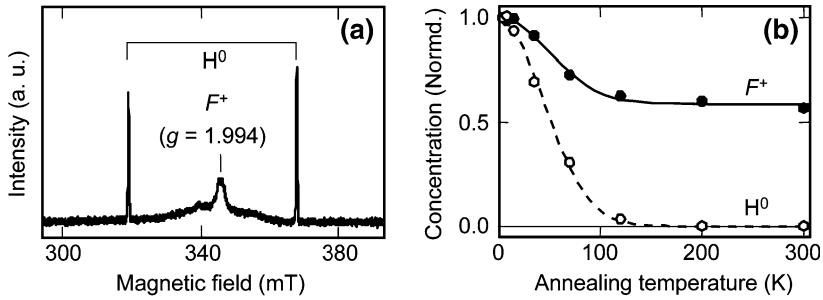

Fig. 9 (**a**) EPR spectra of UV irradiated C12A7:H^- observed at 4 K, revealing a hyperfine doublet structure due to an H^0 and a broad singlet band due to the F^+ center. (**b**) Isochronal annealing of H^0 and F^+. H^0 was completely annihilated above ~200 K, while ~60% of the F^+ centers remain even at 300 K

EPR measurements of the UV-illumination of C12A7:H^- at low temperature reveal that nearly equal amounts of H^0 and F^+-like centers are generated in the C12A7:H^- cage (Fig. 9) [33]. Furthermore, the H^0 concentration was found to decrease abruptly with increasing temperature and disappeared completely above ~100 K. While at the same temperature, the concentration of F^+-like centers decreased modestly, but survived above room temperature. These observations provide strong justification for the photo-dissociation reaction given by Eq. 3, and the dissociation of H^0 given by Eqs. 4 and 5. Observed chemical processes described by these equations provide clear evidence for the presence of an H^- ion in C12A7.

The summation of Eqs. 3–5 gives a reaction that generates two electrons from a single H^- ion:

$$H^-(\text{cage}) + O^{2-}(\text{cage}) + \text{null (cage)} \leftrightarrow 2e^-(\text{cage}) + OH^-(\text{cage}) \quad (6)$$

The validity of this reaction was confirmed by an experimental study of the high-temperature electrical conductivity of C12A7:H^-, and a theoretical analysis [34]. It was found that C12A7:H^- without the UV-illumination exhibits an electrical conductivity about two-orders of magnitude larger than that expected from the oxide ion conductivity below ~550 °C, where C12A7 retains H^- ions stably. Thus, the most likely conduction carriers in this system are thermally generated electrons emitted from the H^- ions. The enthalpy change in the equilibrium reaction of Eq. 6, which is a most provable reaction to generate electrons, is estimated from the apparent activation energy for carrier electron generation (~0.7 eV) to be 1.4 eV (Fig. 10a). On the other hand, theoretical calculations indicate that the energy required for the thermal dissociation of H^- into H^0 and an electron (Eq. 3) is ~3.5 eV, which is much larger than the observed activation energy. However, if H^0 is further decomposed to form an OH^- ion and an electron, the energy gain for the reaction is ~2.5 eV. Consequently, the total energy difference in the equilibrium reaction (Eq. 6), is calculated to be ~1.0 eV, which agrees well with the experimentally obtained enthalpy change (~1.4 eV) (Fig. 10b). Thus, the equilibrium reaction of Eq. 6 provides a sound explanation for the thermal generation of the carrier electrons.

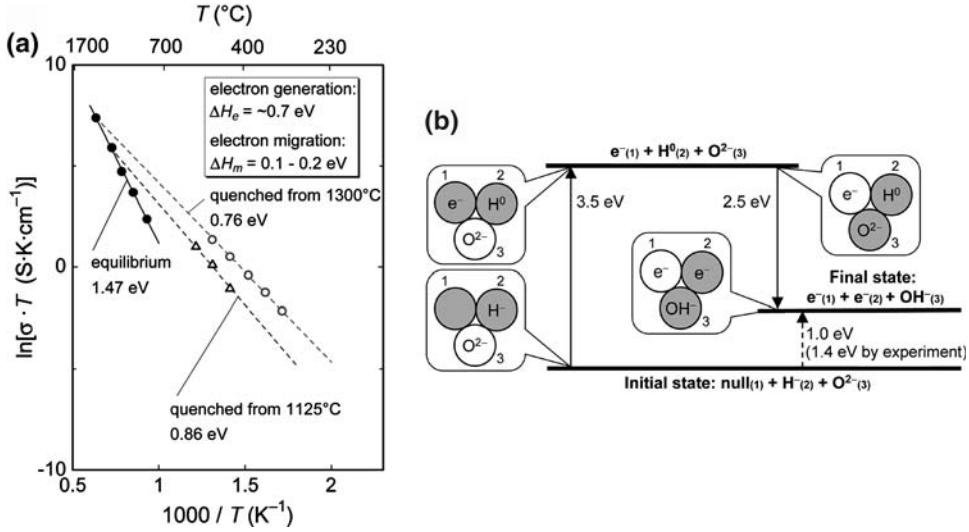

Fig. 10 (**a**) Electrical conductivity of C12A7 in equilibrium with 0.2 atm H_2 (solid line), and of quenched C12A7 (dashed lines). (**b**) Assessment of the energy change associated with the internal equilibrium using theoretical calculations. The illustrations schematically show the cage and extra-framework species. The calculations are performed for configurations composed of two shaded cages in each energy level

The conductive state of C12A7:H^- resulting from the photo-irradiation is also ascribed to the two-electron generation and proton from H^-, which is completed by OH^- ion formation (Eq. 6). According to the scheme of Fig. 10b, the persistence of the photo-induced conductive state is understood by the presence of a high potential barrier for the reverse reaction.

Formation of stable electrides

C12A7 electride

An electride is a crystalline ionic salt in which electrons serve as anions. Typical examples of electrides include compounds of complexant cations (e.g., Cs^+ and crown-ethers) and electron anions [35]. Although electrides are expected to have novel applications due to their exotic characteristics, such as small work functions, they are not stable at room temperature and/or in atmospheres bearing water and/or oxygen. Thus, since the first discovery of electrides by Dye in 1983 [35], intensive efforts have been made to establish synthetic routes suitable for the formation of stable electrides. The first thermally and chemically stable electride was realized in C12A7 [36]. Here, the extra-framework O^{2-} ions are removed from the cages by heating together a single crystal of C12A7 with calcium metal in an evacuated silica glass ampoule. This reaction leads to the formation of high-density (on the order of 10^{21} cm^{-3}) electrons semi-confined to the cages (Fig. 11). The resultant C12A7 may be described as ~$[Ca_{24}Al_{28}O_{64}]^{4+}\cdot 4e^-$, i.e., a C12A7 electride. The electrons localize in the C12A7 cages to form F^+-like centers, thereby behaving as anions in the system. These electrons are able to migrate by hopping to neighboring cages, yielding electrical conductivities as high as ~100 S cm^{-1}. Furthermore, these electrons are coupled antiferromagnetically, forming a diamagnetic pair or a singlet bi-polaron.

Synthesis of C12A7 electride

We have developed three different processes for preparing the C12A7 electride: thermal annealing of single-crystal C12A7 with calcium metal vapor [36], direct solidification of a C12A7 melt in a carbon crucible [37], and hot ion implantation of inert gas ions into C12A7 [38] (described in section 5.4).

Annealing with calcium metal vapor

Figure 11 shows spectra indicating distinct changes in the optical absorption properties and temperature dependences of the electric conductivity of a C12A7 single crystal with annealing time in calcium metal vapor at 700 °C. Here, the electrical conductivity of the C12A7 single crystal at room temperature increased over time, with a simultaneous enhancement of the absorption bands at 2.8 eV and 0.4 eV. These results indicate that the electron concentration in C12A7 increases with annealing time. Interestingly, the electron concentration reaches on the order of 10^{21} cm^{-3} when the crystal is subject to chemical treatment for 240 h, corresponding to an almost complete replacement of the free oxygen with electrons. That is, the C12A7 electride was formed by annealing C12A7 single crystals in calcium metal vapor at 700 °C. It is worth mentioning here that the type of electrical conductivity changes from semiconductor to degener-

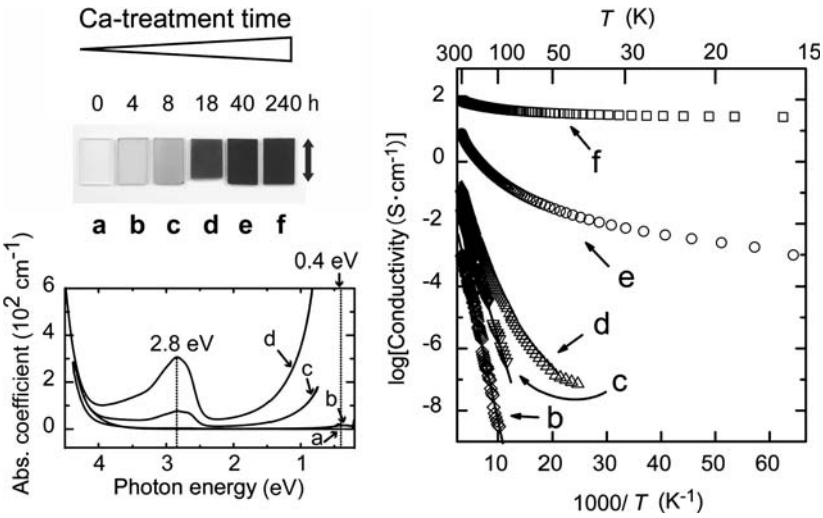

Fig. 11 Images revealing the coloration of C12A7 single crystals processed by Ca-vapor annealing over time. Their corresponding optical absorption spectra (left), and electrical conductivities as a function of temperature (right) are also shown

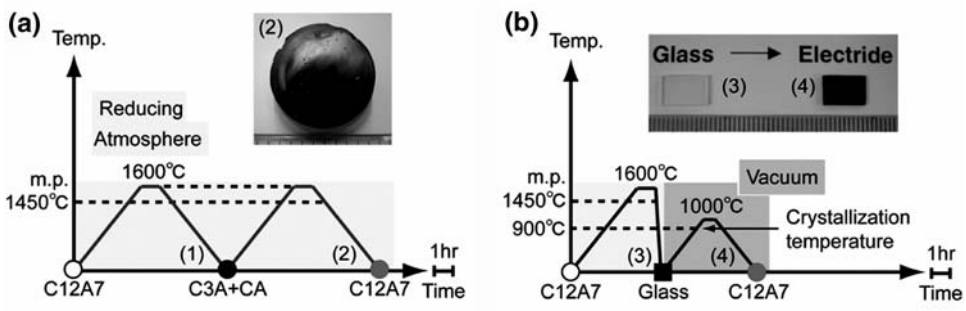

Fig. 12 Fabrication processes for the formation of polycrystalline C12A7 electrides via C12A7 reduced melts or reduced glass. (**a**) Solidification of a reduced C12A7 melt in a carbon crucible. (**b**) Crystallization of the transparent reduced glass under vacuum

ated conduction types with an increase in electron concentration. As such, even metallic conduction is apparent in C12A7 electrides which have an extremely high electron concentration.

Solidification of C12A7 melt in reduced atmosphere

When a mixture of C3A and CA was melted at ~1600 °C in a sealed carbon crucible and then cooled to room temperature in air, the melt solidified to form a dark green electrically conductive C12A7 bulk (Fig. 12a) [37]. Electron formation was confirmed by both optical absorption and EPR studies. Thus, direct solidification in a carbon crucible provides a simple process for the fabrication of polycrystalline C12A7 electrides in large volume, although the complete replacement of 'free oxygen' with electrons is very difficult to achieve. In this process, it is likely that C_2^{2-} ions act as nuclei (templete) for the formation of the C12A7 crystalline phase. During the cooling stage, these C_2^{2-} ions are spontaneously released from the solidified C12A7, leaving behind electrons in the cages. Further, rapid quenching of a melt with stoichiometric composition of C12A7 results in formation of insulating transparent C12A7 glass. Its crystallization in vacuum also affords an electrically conductive C12A7 bulk (Fig. 12b). This result supports the assumption that the C_2^{2-} ions play a significant role in the formation of electrons.

Electron emission from C12A7 electride

We investigated the electric-field electron emission from the C12A7 electride under vacuum [39,40]. The measured electron emission properties have been explained by Fowler–Nordheim tunneling at high electric fields (>200 kV cm^{-1}), and thermionic emission at lower electric fields. The work function estimated from the emission characteristics (~0.6 eV) is comparable to those reported for conventional organic electrides. However, ultraviolet photoelectron spectroscopy gave a much larger value (~2.4 eV) for the work function. This discrepancy may be attributed to the surface band bending effect due to the n^+/n^- layers formed by oxidation of the electride surface. Based on the field emission of electrons from the electride at room temperature, a triode-structured field emission device was fabricated in which the electride was employed as a cathode and a ZnO:Zn green phosphor plate as an anode. Cathode luminescence was clearly observed under typical ambient light, demonstrating that the C12A7 electride shows distinct promise for application in field emission display (FED) devices (Fig. 13).

Recently, we have examined the thermal field emission (TFE) from a sharpened C12A7 electride single crystal for applied external voltages of 0–6 kV, at temperatures up to 900 (C in a 10^{-5} Pa vacuum, using the setup shown in Fig. 14a [40]. Here, TFE started to occur at ~600 °C, and at more elevated temperatures (~900 °C), the current was observed to rise steeply, reaching >80 μA (1.5 A cm^{-2}). The emission from a 80-μm-diameter area obtained with a

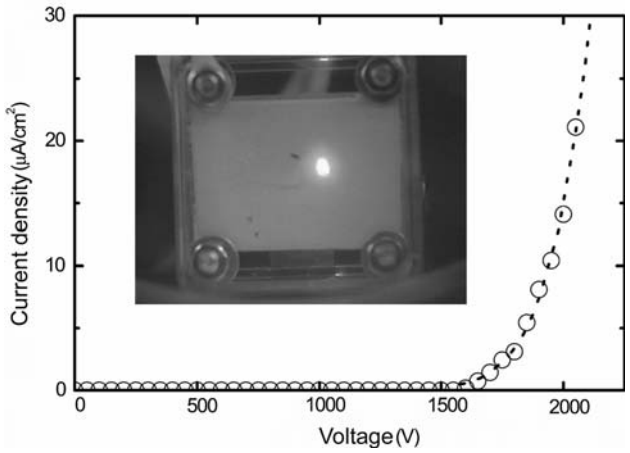

Fig. 13 Current-voltage characteristics representing electron emission from a single crystal C12A7 electride. The inset is a photograph showing the operation of a field-emission light-emitting device using a ZnO:Zn phosphor

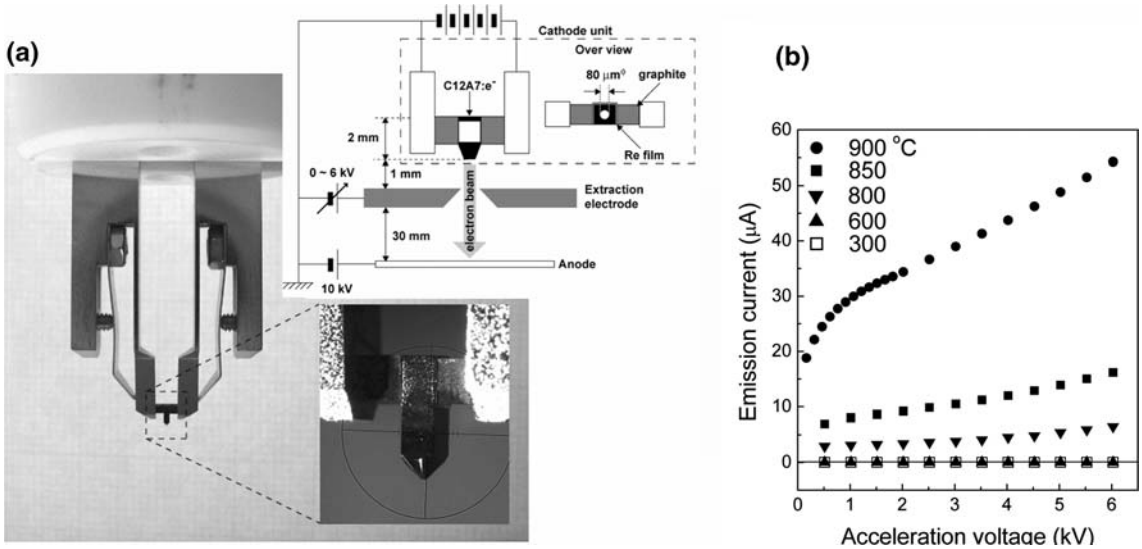

Fig. 14 Thermal field emission (TFE) from a C12A7 electride (**a**) Experimental setup for measuring TFE. The two photographs show the TFE head equipped with an emission tip prepared from a C12A7 single crystal. (**b**) Electron emission current as a function of extraction voltage at several temperatures

current of ~50 μA was sustained stably for more than 90 h in an extraction field of 10^5 V cm^{-1} (Fig. 14b). The work function estimated using the Richardson–Dushman equation was ~2.1 eV, which is smaller than that of LaB_6 (~2.7 eV). These experiments demonstrate that the C12A7 electride has a high potential for both cold electron emission and TFE applications. The different characteristics of the two modes of electron emission are likely due to the difference in the surface state of the C12A7 electride.

Hot-ion implantation

The fabrication of good C12A7:H^- and C12A7 electride thin films is a major requisite for many device applications. Here, we succeeded in incorporating H^- ions and electrons into C12A7 films by the hot implantation of H^+ and inert gas ions [27]. UV light illumination of the resulting H^+-ion-implanted films induced the electrically conductivity and forms of F^+-like centers. This observation confirms that the H^- ions were formed by proton implantation. The UV-induced electron concentration increased with increasing substrate temperature during the implantation, where the optimum temperature for H^- formation was 600–700 °C. This process also affords to control the electrical conductivity after UV illumination through the fluences of the implanted ions. For example, fluences of 1×10^{18} cm^{-2} gave electrical conductivity values of ~10 S cm^{-1} at room temperature.

To our surprise, the heavy implantation of inert gas ions into C12A7 resulted in electron carrier generation. Inert gas ion (Ar^+, He^+) implantation into C12A7 films, with fluences from 1×10^{16} to 1×10^{17} cm^{-2} at an elevated temperature of 600 °C [38], yielded colored films that exhibited high electrical conductivities in the as-implanted state (Fig. 15). This result may be explained from the removal of the extra-framework O^{2-} ions due to the 'kick-off effect' caused by the implanted inert gas ions, leaving behind electrons in the cages. The induced electron concentration is proportional to the

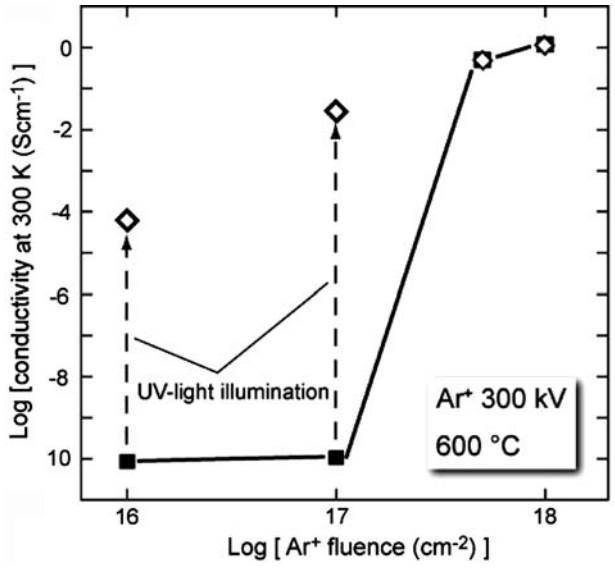

Fig. 15 Ar^+-dose dependence of electrical conductivity in implanted C12A7 films. Filled squares and open rhombuses indicate electrical conductivities before and after UV-light irradiation, respectively

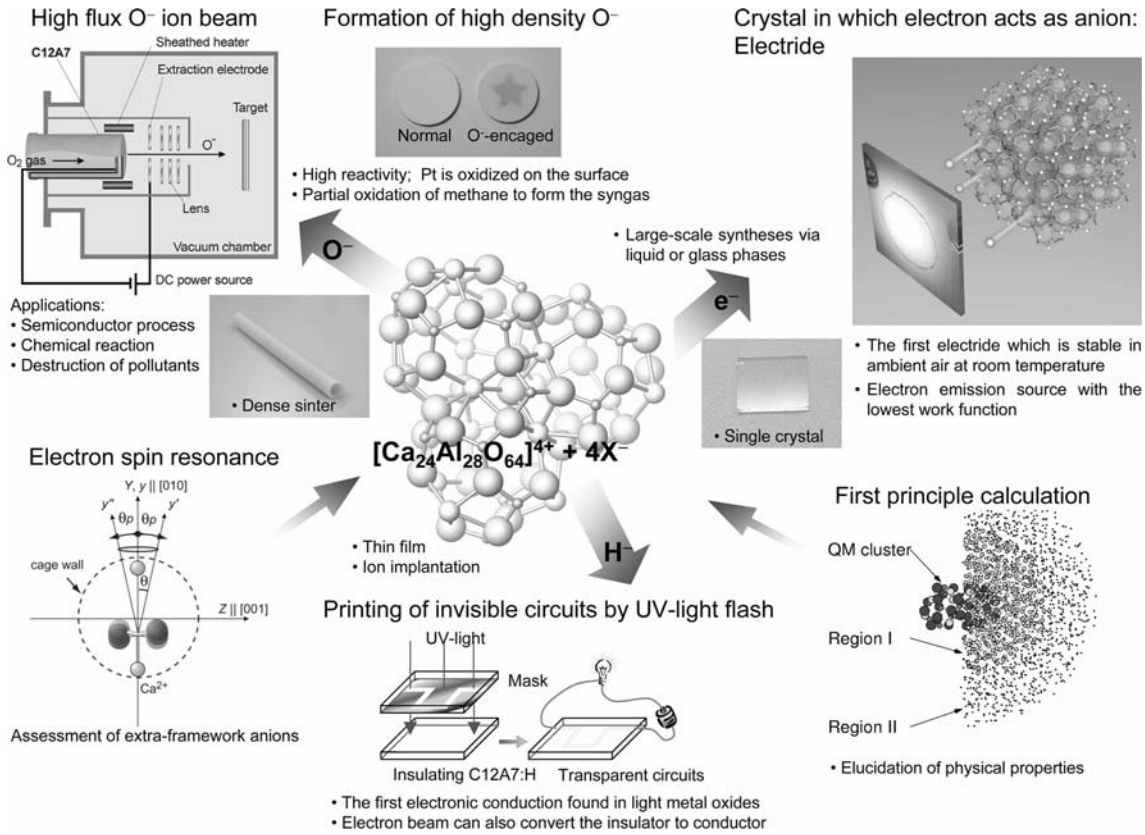

Fig. 16 Current status of active functionalities realized in $12CaO{\cdot}7Al_2O_3$ (C12A7)

displacements per atom (dpa; 1 dpa means all atoms in the projected range are displaced once), suggesting that the nuclear collision effect of the implanted ions plays a dominant role in the removal of the O^{2-} ions. On the other hand, when the fluence was less than 1×10^{17} cm^{-2}, the transparent and insulating as-implanted films exhibited coloration and electrical conductivity upon illumination with UV light, suggesting that H^- ions were formed by the inert gas implantation. Based on the decrease in OH^- concentration within the C12A7 films after implantation, it is likely that preexisting OH^- ions in the cages may be converted to H^- ions due to the implantation. The hot-ion implantation technique provides a novel physical process for preparing electrically conductive C12A7 films.

Concluding remarks

The results described in this article are summarized in Fig. 16. The functionalities shown here can be realized only from commonplace materials, such as CaO, Al_2O_3 and H_2O. The constitutional elements of C12A7 (i.e., Ca, Al and O) are ranked among the top five most abundant elements within the Earth's crust. It is our belief that the present study is a representative case study exploring novel functional materials composed of these abundant elements. It is remarkable that active anionic species such as O^-, H^-, and electrons, can be stabilized simply by incorporating them into a positively-charged lattice framework. Active use of nanostructures in the framework, periodically distributed nano-size cages, leads to the creation of novel properties such as high oxidation reactivity, an electronic insulator-conductor conversion mediated by light-illumination, and the realization of electrides that are stable in ambient air at room temperature. These results represent promising findings for realizing future practical applications, such as improvements to cold cathode electron emission displays, and the potential development of an O^- ion beam gun that continuously emits an intense high purity O^- ion beam.

Acknowledgements We appreciate our collaborators, Drs. Satoru Matsuishi, Masashi Miyakawa, Sung-Wng Kim, Yoshikake Toda and Toshio Kamiya of Tokyo Institute of Technology, Drs. Peter V. Sushko and Alexander L. Shluger of University College London, and Dr. Isao Tanaka of Yamanashi University. This work is supported by a Grant-in-Aid for Creative Research (No.16GS0205) from the Japanese Government MEXT, and in part by a Grant-in-Aid for Industrial Technology Research (No. 05A25513a) from NEDO. A part of the research

was performed within the framework of the ERATO program run by the Japan Science and Technology Agency.

References

1. Bartl HB, Scheller T (1970) Neues Jahrb Mineral Monatsh 35:547
2. Nurse RW, Welch JH, Majumdar A (1965) Trans Br Ceram Soc 64:323
3. Jeevaratnam J, Glasser FP Glasser LSD (1964) J Am Ceram Soc 47:105
4. Hosono H, Abe Y (1987) Inorg Chem 26:1192
5. Lacerda M, Irvine JTS, Glasser FP, West AR (1988) Nature 332:525
6. Hosono H, Yamazaki K, Abe Y (1987) J Am Ceram Soc 70:867
7. Hosono H, Asada N, Abe Y (1990) J Appl Phys 67:2840
8. Hosono H (2004) Int J Appl Ceram Tech 5:409
9. Kamiya T, Hosono H (2005) Jpn J Appl Phys 44:774
10. Hayashi K, Hirano M, Hosono H (2002) J Mater Res 17:1244
11. Watauchi S, Tanaka I, Hayashi K, Hirano M, Hosono H (2002) J Cryst Growth 237:496
12. Toda Y, Miyakawa M, Hayashi K, Kamiya T, Hirano M, Hosono H (2003) Thin Solid Films 445:309
13. Hayashi K, Hirano M, Matsuishi S, Hosono H (2002) J Am Chem Soc 124:736
14. Hayashi K, Matsuishi S, Ueda N, Hirano M, Hosono H (2003) Chem Mater 15:1851
15. Hayashi K, Hirano M, Hosono H (2005) J Phys Chem B 109:11900
16. Yang S, Kondo JN, Hayashi K, Hirano M, Domen K, Hosono H (2003) Chem Mater 16:104
17. Hayashi K, Hirano M, Hosono H (2005) Chem Lett 34:586
18. Hayashi K, Matsuishi S, Hirano M, Hosono H (2004) J Phys Chem B 108:8920
19. Hayashi K, Ueda N, Hirano M, Hosono H (2004) Solid State Ionics 179:89
20. Matsuishi S, Hayashi K, Hirano M, Tanaka I, Hosono H (2004) J Phys Chem B 108:8920
21. Yang S, Kondo JN, Hayashi K, Hirano M, Domen K, Hosono H (2004) Appl Catal A 277:234
22. Li Q, Hayashi K, Nishioka M, Kashiwagi H, Hirano M, Torimoto Y, Hosono H, Sadakata M (2002) Appl Phys Lett 80:4259
23. Hayashi K, Hirano M, Li Q, Nishioka M, Sadakata M, Torimoto Y, Matsuishi S, Hosono H (2002) Electorochem Solid State Lett 5:J13
24. Li Q, Hayashi K, Nishioka M, Kashiwagi H, Hirano M, Torimoto Y, Hosono H, Sadakata M (2002) Jpn J Appl Phys 41:L530
25. Li Q, Hosono H, Hirano M, Hayashi K, Nishioka M, Kashiwagi H, Torimoto Y, Sadakata M (2003) Surf Sci 527:100
26. Hayashi K, Matsuishi S, Kamiya T, Hirano M, Hosono H (2002) Nature 419:462
27. Miyakawa M, Hayashi K, Hirano M, Toda Y, Kamiya T, Hosono H (2003) Adv Mater 15:1100
28. Hayashi K, Toda Y, Kamiya T, Hirano M, Yamanaka M, Tanaka I, Yamamoto T, Hosono H (2005) Appl Phys Lett 86:22109
29. Sushko PV, Shluger AL, Hayashi K, Hirano M, Hosono H (2003) Phys Rev Lett 91:126401
30. Sushko PV, Shluger AL, Hayashi K, Hirano M, Hosono H (2003) Thin Solid Films 445:161
31. Sushko PV, Shluger AL, Hayashi K, Hirano M, Hosono H (2005) Mater Sci Eng C 25:722
32. Sushko PV, Shluger AL, Hayashi K, Hirano M, Hosono H (2005) Appl Phys Lett 86:92101
33. Matsuishi S, Hayashi K, Hirano M, Hosono H (2005) J Am Chem Soc 127:12454
34. Hayashi K, Sushko PV, Shluger AL, Hirano M, Hosono H (2005) J Phys Chem B 109:11900
35. Dye L (1997) Inorg Chem 36:3817
36. Matsuishi S, Toda Y, Miyakawa M, Hayashi K, Hirano M, Tanaka I, Hosono H (2003) Science 301:626
37. Kim S-W, Miyakawa M, Hayashi K, Sakai T, Hirano M, Hosono H (2005) J Am Chem Soc 127:1370
38. Miyakawa M, Toda Y, Hayashi K, Kamiya T, Hirano M, Matsunami N, Hosono H (2005) J Appl Phys 97:23510
39. Toda Y, Matsuishi S, Hayashi K, Ueda K, Kamiya T, Hirano M, Hosono H (2004) Adv Mater 16:685
40. Toda Y, Kim S-W, Hayashi K, Hirano M, Kamiya T, Hosono H, Haraguchi T, Yasuda H (2005) Appl Phys Lett 87:254103